Active Deformation Control for a Magnetically Levitated Planar Motor Mover

Ioannis Proimadis, Coen H. H. M. Custers, *Member, IEEE*, Roland Tóth, *Senior Member, IEEE*, J. W. Jansen, Hans Butler, Elena Lomonova, *Senior Member, IEEE*, and Paul M. J. Van den Hof, *Fellow, IEEE*

***Abstract*—This article describes a method for the active control of the deformations on a magnetically levitated moving-magnet planar motor. The planar motor under consideration is comprised of a stator on a double coil array configuration and a mover with permanent magnets, and it is designed to perform positioning tasks with nanometer level of accuracy. Due to the spatially asymmetric, nonuniform force distribution on the magnet plate, mechanical deformations are induced to the mover, which can severely hinder the desired positioning accuracy. The proposed method overcomes this challenge by properly shaping the force distribution on the moving magnet plate, which is enabled by the presence of multiple coils interacting with the mover, corresponding to an "overactuation" scheme. As a consequence, the independent control of elementary deformation shapes (modes) is achieved. The proposed overactuation scheme is experimentally validated on a planar motor prototype, proving the efficiency of the proposed method during both standstill and motion.**

***Index Terms*—Control engineering, motion control, permanent magnet motors.**

I. Introduction

MOTION systems are mechanical devices tailored to perform positioning tasks. They are utilized in a wide range of applications, from high-resolution microscopes to product inspection machines and medical devices. A state-of-the-art application where motion systems play a crucial role are wafer scanners, which are complex machines used in the semiconductor industry to manufacture integrated circuits by lithography. In these machines, the wafer stage is a motion system, which is responsible for positioning a silicon wafer at a given location, based on a motion pattern, where a light beam creates a pattern on the wafer.

Recent expectations for wafer stages include both high positioning accuracy ($<10^{-9}$ m) and high accelerations of more than 50 $\mathrm{m/s^2}$. Toward realizing these challenging goals, modern wafer stages rely on the use of double-stroke planar motors [1], [2]. In these designs, moving-coil magnetically levitated motors are utilized for the long-range motion, while both the stability and the propulsion of the mover is provided by means of magnetic fields [3]. On top of this motor voice-coil actuators are used for the short-stroke, high precision motion. Such configurations usually lead to bulky, complex, and expensive systems. Moreover, the physical connection of the mover with the environment through a cable slack, which is required to provide power to the coils and the cooling system, results in disturbances on the wafer stage that limit the achievable performance. Toward overcoming the aforementioned challenges, alternative planar motor configurations have also been investigated in the recent years, which rely on a magnetically levitated, single-stroke, moving-magnet motor configuration [4]–[8]. In this design, the mover is in principle a freely floating body with no physical connection to the environment, thereby limiting the effect of environmental disturbances on the mover.

The constant demand for higher actuation bandwidth in wafer stages, in combination with the limited mechanical stiffness of the mover in the aforementioned motor configurations bring into light the flexible dynamics of the mover [9], [10]. As a result, the spatially nonuniform distribution of force on the mover induces mechanical deformations, which can severely limit the attained positioning accuracy [11], [12]. Toward suppressing their effect two classes of approaches exist. Passive techniques aim at modifying the mechanical properties of the plant, such that the resulting system achieves higher stiffness, damping, and isolation of the vibrations. Active methods modify the behavior of the system by shaping the closed-loop behavior of the system, i.e., through appropriate control design. Depending on the problem at hand, each approach or a combination of the two can be of use.

Manuscript received February 7, 2021; revised June 10, 2021; accepted August 10, 2021. Date of publication October 11, 2021; date of current version January 14, 2022. Paper 2021-EMC-0072.R1, presented at the 2019 IEEE International Electric Machines and Drives Conference, San Diego, CA, USA, May 12–15, and approved for publication in the IEEE TRANSACTIONS ON INDUSTRY APPLICATIONS by the Electric Machines Committee of the IEEE Industry Applications Society. This work was supported in part by the Dutch Organization for Scientific Research (NWO, domain TTW Grant 13320), which is partly funded by the Ministry of Economic Affairs of The Netherlands, and in part by the Ministry of Innovation and Technology NRDI Office within the framework of the Autonomous Systems National Laboratory Program. *(Corresponding author: Ioannis Proimadis.)*

Ioannis Proimadis and Paul M. J. Van den Hof are with the Control Systems Group, Department of Electrical Engineering, Eindhoven University of Technology, 5600 MB Eindhoven, The Netherlands (e-mail: jproimadis@gmail.com; p.m.j.vandenhof@tue.nl).

Coen H. H. M. Custers, J. W. Jansen, and Elena Lomonova are with the Electromechanics and Power Electronics Group, Department of Electrical Engineering, Eindhoven University of Technology, 5600 MB Eindhoven, The Netherlands (e-mail: c.h.h.m.custers@tue.nl; j.w.jansen@tue.nl; e.lomonova@tue.nl).

Roland Tóth is with the Control Systems Group, Department of Electrical Engineering, Eindhoven University of Technology, 5600 MB Eindhoven, The Netherlands, and also with Systems and Control Laboratory, Institute for Computer Science and Control, H-1111 Budapest, Hungary (e-mail: r.toth@tue.nl).

Hans Butler is with the Control Systems Group, Department of Electrical Engineering, Eindhoven University of Technology, 5600 MB Eindhoven, The Netherlands, and also with ASML, 5504 DR Veldhoven, The Netherlands (e-mail: h.butler@tue.nl).

Color versions of one or more figures in this article are available at https://doi.org/10.1109/TIA.2021.3119005.

Digital Object Identifier 10.1109/TIA.2021.3119005

An often followed active approach is based on overactuation. In motion systems, this term is coined to describe the case where the number of actuators is higher than the number of rigid-body degrees of freedom (DOFs). In such systems, a typical control strategy is based on the active control of the rigid-body behavior, while the flexible behavior is suppressed via the proper design of the feedback controller [13]. However, in an overactuation scheme, it is possible to realize additional independent control of the flexible behavior next to controlling the rigid-body DOFs. In practice, active control of the deformation is achieved by first describing it as a summation of elementary motions, called modes [14], and subsequently shaping the force distribution on the mover such that a collection of modes (e.g., the most dominant ones) are independently controlled.

The first publications regarding the use of the overactuation scheme for the control of planar motion systems have been reported in [15] and [16] together with experimental results in [9] and [17]. In these works, overactuation has been exploited for the design of feedback controllers. Moreover, in [18], a data-based while, in [19], a model-based approach has been applied for active feedforward control of flexible modeshapes.

In the aforementioned publications, the investigated system is based on short-stroke, voice-coil actuators. For the long-stroke magnetically levitated planar motors, the main challenge toward overactuation lies in the fact that the exerted forces on the mover are produced by means of electromagnetic fields, whose characteristics heavily depend, in a nonlinear fashion, on the relative position between the magnets and the coils. Moreover, in the moving-coil configuration, the location of the exerted forces on the mover is fixed with respect to the center of mass. On the contrary, in the moving-magnet configuration, the produced forces are spatially distributed over the flexible mover, while the characteristics of this spatial distribution depend nonlinearly on the relative position of the mover. As a result, imposing the desired force distribution on the moving-magnet topology requires additional considerations, compared to the moving-coil configuration.

In this publication, the overactuation scheme for moving-magnet planar motors is developed and experimentally validated. To achieve this, the dynamic model that describes the position-dependent electromagnetic and mechanical phenomena is introduced first. Using this model, the relation between the current distribution in the coils and the resulting excitation of specific flexible modes is established. By exploiting this relation, a methodology is developed which enables the independent control for a number of flexible modes, in addition to the rigid-body modes. The developed framework is experimentally validated on the double layer planar motor (DLPM) prototype [20], which is a single-stage, long-stroke synchronous motor, capable of moving in all 6 rigid-body DOFs with high accuracy. This motor is a viable alternative to the state-of-the-art motion systems, and therefore, overactuation can be of vital importance toward achieving nanometer positioning accuracy.

This article is organized as follows. The main properties of the DLPM prototype are discussed in Section II, together with the control architecture. In Section III, the overactuation scheme is analyzed. The developed scheme is experimentally validated, and the associated results are discussed in Section IV. Finally, conclusions are drawn in Section V.

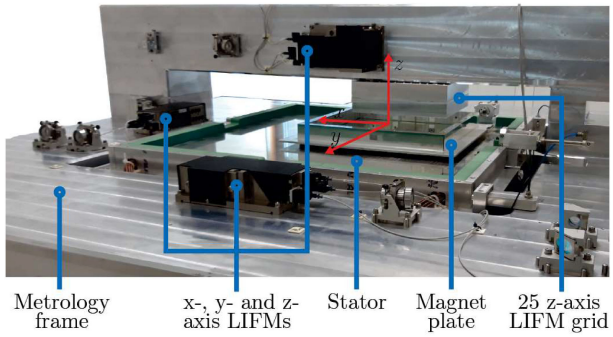

Fig. 1. DLPM prototype, with the main components being highlighted.

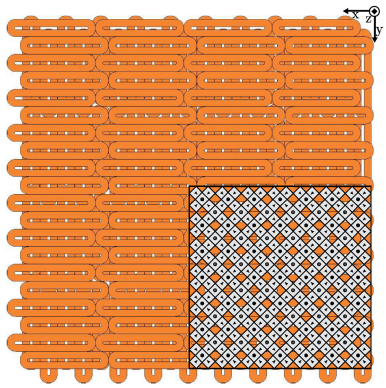

Fig. 2. Double-layer coil array and magnet plate (shown in bottom right) of the DLPM prototype.

II. Double Layer Planar Motor

A. Motor Design

The DLPM prototype, shown in Fig. 1, consists of three main frames, namely the stator, the magnet plate, and the metrology frame. In the stator, shown in Fig. 2, the 160 coils are placed in a double array configuration and they are responsible for the levitation and propulsion of the magnet plate. The top-layer coils provide the force in the y- and z-directions, while the bottom coils in the x- and z-directions. The actuation of the coils is accomplished through the use of 40 single-phase power amplifiers. To each amplifier, four different coils are connected via a multiplexer. The coils are located on the four quadrants of the coil array, and a switching mechanism selects the closest coil to the magnet plate at a given time instant. In this way, the independent control of 40 coils is accomplished. The stator lies on a concrete base, and its top surface defines the operating region for the freely floating magnet plate. The magnet array is located on the bottom of the mover and it consists of 281 magnets in quasi-Halbach configuration [21], while the side and top surface of the mover are covered with mirrors. The overall design of the motor has been optimized in terms of force production, power losses and mechanical deformations [7], [11], resulting in the selection of the coil and magnet dimensions detailed in [6] and [22].

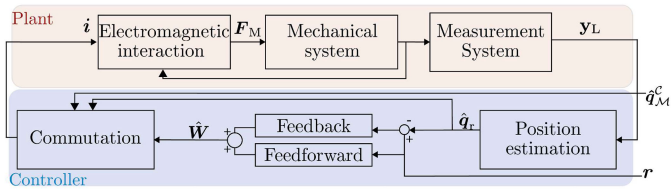

Fig. 3. Block diagram for the DLPM prototype. The top area corresponds to the plant motor system and the bottom area to the controller structure.

The stator is surrounded by the metrology frame, on which the measurement devices are mounted. The main measurement system consists of nine laser interferometers (LIFMs), which provide information regarding the displacement of the mover in all three principal directions and they are used in closed loop for the estimation of the rigid-body configuration. Additionally, an auxiliary 25-LIFM system, positioned on a 5×5 grid, provides information about the displacement of the plate in the z-direction. Moreover, a set of eddy current sensors measures the relative position between the metrology and the stator. Finally, the metrology frame rests upon four air-mounts, which act as low-pass filters, thereby suppressing the influence of floor vibrations on the measurement system.

B. Operating Principles

1) Overview: The operating principles of the magnetically levitated planar motor are characterized by the series interconnection of three subsystems, as shown in Fig. 3. First, the electromagnetic principles describe how the interaction between the controlled current in the coils and the magnets result in a force distribution on the magnet plate. The mechanical principles describe how these forces result in the motion of the magnet plate. The displacement is measured by the 9-LIFM system and the information is supplied to the controller.

2) Electromagnetic Principles: The electromagnetic interaction is described using the Lorentz force law [21]. Under the rigid-body assumption, the total force and torque acting on the mover is equal to the sum of the individual force and torque contributions of the 40 active coils. By defining the total force (F) and torque (τ) on the three principal axes as

$$\boldsymbol{W} = \begin{bmatrix} F_x & F_y & F_z & \tau_x & \tau_y & \tau_z \end{bmatrix}^\top \tag{1}$$

the relation between the supplied currents and the resulting force and torque components, under the rigid-body assumption, is given by

$$\boldsymbol{W} = \underbrace{\begin{bmatrix} M^1_{F_x}\left(\boldsymbol{q}^{\mathcal{C}}_{\mathcal{T}}\right) & \cdots & M^{n_c}_{F_x}\left(\boldsymbol{q}^{\mathcal{C}}_{\mathcal{T}}\right) \\ M^1_{F_y}\left(\boldsymbol{q}^{\mathcal{C}}_{\mathcal{T}}\right) & \cdots & M^{n_c}_{F_y}\left(\boldsymbol{q}^{\mathcal{C}}_{\mathcal{T}}\right) \\ M^1_{F_z}\left(\boldsymbol{q}^{\mathcal{C}}_{\mathcal{T}}\right) & \cdots & M^{n_c}_{F_z}\left(\boldsymbol{q}^{\mathcal{C}}_{\mathcal{T}}\right) \\ M^1_{\tau_x}\left(\boldsymbol{q}^{\mathcal{C}}_{\mathcal{T}}\right) & \cdots & M^{n_c}_{\tau_x}\left(\boldsymbol{q}^{\mathcal{C}}_{\mathcal{T}}\right) \\ M^1_{\tau_y}\left(\boldsymbol{q}^{\mathcal{C}}_{\mathcal{T}}\right) & \cdots & M^{n_c}_{\tau_y}\left(\boldsymbol{q}^{\mathcal{C}}_{\mathcal{T}}\right) \\ M^1_{\tau_z}\left(\boldsymbol{q}^{\mathcal{C}}_{\mathcal{T}}\right) & \cdots & M^{n_c}_{\tau_z}\left(\boldsymbol{q}^{\mathcal{C}}_{\mathcal{T}}\right) \end{bmatrix}}_{M^{\mathrm{r}}\left(\boldsymbol{q}^{\mathcal{C}}_{\mathcal{T}}\right)} \underbrace{\begin{bmatrix} i_1 \\ \vdots \\ i_{n_c} \end{bmatrix}}_{\boldsymbol{i}} \tag{2}$$

where $\boldsymbol{i}$ denotes the current vector, which contains the current values supplied to the $n_c = 40$ active coils. Moreover, the matrix $M^{\mathrm{r}} \in \mathbb{R}^{n_r \times n_c}$ collects the individual current to force/torque coefficients, with $n_r = 6$ denoting the number of rigid-body modes. These coefficients depend on the relative position of the translator (magnet plate) frame $\mathcal{T}$ with respect to the coil frame $\mathcal{C}$, denoted as $\boldsymbol{q}^{\mathcal{C}}_{\mathcal{T}} \in \mathbb{R}^{n_r}$.

3) Mechanical Principles and Measurement System: For the description of the mechanical properties of the mover, both the rigid-body and the flexible-body properties are of relevance. Deriving an analytic expression for the motion dynamics for complex structures, such as the magnet plate, is a laborious or even impossible task. Instead, a solution is derived by resorting to the finite element method approach, which numerically approximates the dynamic behavior of the system on a user-defined finite set of spatial coordinates.

By denoting with $\boldsymbol{F}_{\mathrm{M}}$ the force vector and $\mathbf{y}_{\mathrm{L}}$ the measurement vector, using the 9-LIFM system, the derived dynamics in the modal form [14] are described by the state-space model

$$\begin{aligned} \frac{d}{dt}\begin{bmatrix} \boldsymbol{q}_{\mathrm{r}} \\ \boldsymbol{q}_{\mathrm{f}} \\ \dot{\boldsymbol{q}}_{\mathrm{r}} \\ \dot{\boldsymbol{q}}_{\mathrm{f}} \end{bmatrix} &= \left[\begin{array}{c|c} 0_{n_m \times n_m} & I_{n_m} \\ \hline \begin{bmatrix} 0_{n_{\mathrm{r}} \times n_{\mathrm{r}}} & 0_{n_{\mathrm{r}} \times n_{\mathrm{f}}} \\ 0_{n_{\mathrm{f}} \times n_{\mathrm{r}}} & -\Omega^2 \end{bmatrix} & \begin{bmatrix} 0_{n_{\mathrm{r}} \times n_{\mathrm{r}}} & 0_{n_{\mathrm{r}} \times n_{\mathrm{f}}} \\ 0_{n_{\mathrm{f}} \times n_{\mathrm{r}}} & -2Z\Omega \end{bmatrix} \end{array}\right] \\ &\quad \times \begin{bmatrix} \boldsymbol{q}_{\mathrm{r}} \\ \boldsymbol{q}_{\mathrm{f}} \\ \dot{\boldsymbol{q}}_{\mathrm{r}} \\ \dot{\boldsymbol{q}}_{\mathrm{f}} \end{bmatrix} + \begin{bmatrix} 0_{n_{\mathrm{r}} \times 3n_{\mathrm{M}}} \\ 0_{n_{\mathrm{f}} \times 3n_{\mathrm{M}}} \\ \Phi_{\mathrm{r}}^{\mathbb{I}\top} \\ \Phi_{\mathrm{f}}^{\mathbb{I}\top} \end{bmatrix} \boldsymbol{F}_{\mathrm{M}} \\ \mathbf{y}_{\mathrm{L}} &= \begin{bmatrix} \Phi_{\mathrm{r}}^{\mathbb{O}}\left(\boldsymbol{q}_{\mathrm{r}}\right) & \Phi_{\mathrm{f}}^{\mathbb{O}}\left(\boldsymbol{q}_{\mathrm{r}}\right) & 0_{n_{\mathrm{y}} \times n_{\mathrm{r}}} & 0_{n_{\mathrm{y}} \times n_{\mathrm{f}}} \end{bmatrix} \begin{bmatrix} \boldsymbol{q}_{\mathrm{r}} \\ \boldsymbol{q}_{\mathrm{f}} \\ \dot{\boldsymbol{q}}_{\mathrm{r}} \\ \dot{\boldsymbol{q}}_{\mathrm{f}} \end{bmatrix} \end{aligned} \tag{3}$$

where $\Omega = \mathrm{diag}(\omega_1, \ldots, \omega_{n_{\mathrm{f}}})$, $Z = \mathrm{diag}(\zeta_1, \ldots, \zeta_{n_{\mathrm{f}}}) \in \mathbb{R}^{n_{\mathrm{f}} \times n_{\mathrm{f}}}$ are diagonal matrices with the elements in the brackets placed in the main diagonal. These correspond, respectively, to the resonance frequencies and damping ratios, and they are placed in ascending frequency order. Moreover, 0 and I denote the zero and identity matrices, respectively, with dimensions indicated in the corresponding subscripts. The vector $\boldsymbol{q}_{\mathrm{r}} \in \mathbb{R}^{n_r}$ is defined as

$$\boldsymbol{q}_{\mathrm{r}} = \begin{bmatrix} x & y & z & \chi & \psi & \zeta \end{bmatrix}^\top \tag{4}$$

where x, y, z are the rigid-body displacements of the magnet plate with respect to the metrology (global) reference frame and χ, ψ, ζ are the associated rotations. In a similar fashion, the states in the vector $\boldsymbol{q}_{\mathrm{f}} \in \mathbb{R}^{n_{\mathrm{f}}}$ describe the contribution of the flexible modes, which lead to the deformation of the mover. The total number of modes, n_{m}, is equal to the sum of rigid- and flexible-body modes, $n_{\mathrm{m}} = n_{\mathrm{r}} + n_{\mathrm{f}}$.

Regarding the output equation, the modeshape matrices $\Phi_{\mathrm{r}}^{\mathbb{O}}(\boldsymbol{q}_{\mathrm{r}}) : \mathbb{R}^{n_{\mathrm{r}}} \mapsto \mathbb{R}^{n_{\mathrm{y}} \times n_{\mathrm{r}}}$, $\Phi_{\mathrm{f}}^{\mathbb{O}}(\boldsymbol{q}_{\mathrm{r}}) : \mathbb{R}^{n_{\mathrm{r}}} \mapsto \mathbb{R}^{n_{\mathrm{y}} \times n_{\mathrm{f}}}$ relate the rigid- and the flexible-body states, respectively, to the measurement vector $\mathbf{y}_{\mathrm{L}} \in \mathbb{R}^{n_{\mathrm{y}}}$. Since the location of the LIFMs is fixed as the translator moves, different points of its surface are targeted by the lasers. As a result, the aforementioned modeshape matrices are position-dependent.

TABLE I
RESONANCE FREQUENCIES OF THE MOVER OF THE DLPM PROTOTYPE

Flexible mode	1	2	3	4
Frequency [Hz]	226.5	546.5	698.5	1050

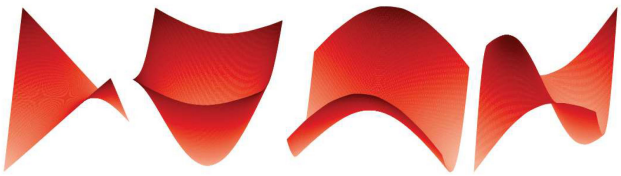

Fig. 4. Illustration of the deformation shape on z-direction of the top surface of the mover. The shapes correspond to the case where only the associated flexible-body state is nonzero. Left to right: flexible modes 1 to 4.

For the actuation part, it was already shown in (2) how the currents are related to the total force and torque vector. Based on the definition of the rigid-body states in (4), using first-principles considerations, the product $\Phi_{\mathrm{r}}^{\mathbb{I}\top}\boldsymbol{F}_{\mathrm{M}}$ can be substituted by $\mathrm{diag}(1/m, 1/m, 1/m, 1/I_x, 1/I_y, 1/I_z)\boldsymbol{W}$ [23], with m denoting the mass and I_x, I_y, I_z the inertia values on the three principal directions. For the flexible part, which manifests itself via the product $\Phi_{\mathrm{f}}^{\mathbb{I}\top}\boldsymbol{F}_{\mathrm{M}}$, the location of the applied forces on the magnet plate has to be defined. Following the discussion in [20], the force vector $\boldsymbol{F}_{\mathrm{M}}$ is defined as the collection of the three-dimensional force components applied at the center of each magnet. As a result, the vector has $3n_{\mathrm{M}}$ elements, where $n_{\mathrm{M}} = 281$ is the number of the magnets.

Based on the discussion mentioned above, the DLPM prototype has been modeled in ANSYS [24] and the results have been used to generate the state-space model (3). The frequencies of the first four flexible modes are shown in Table I, and in total $n_{\mathrm{f}} = 9$ flexible modes have been modeled. The resulting deformation on the top surface of the mover along the z-direction for the first four flexible modes is shown in Fig. 4.

C. Control Architecture and Commutation

The planar motor is an intrinsically unstable system, for which the presence of feedback is necessary for stabilizing the system. Moreover, based on (3), the planar motor exhibits position-dependent dynamics both in the actuation part, as it was shown in (2), as well as in the measurement part. A standard approach for facilitating feedback/feedforward control design at the presence of these phenomena is through the use of first-principles based decoupling and linearization methods, both on the actuation and on the measurement part. These methods aim at reducing coupling between controller inputs and outputs, thus enabling the intuitive design of the dynamic controllers by resorting to single input single output (SISO) loopshaping-based techniques.

By following the aforementioned approach, the resulting controller is composed of four parts, as shown in Fig. 3. The position estimation block estimates the rigid-body states using geometric considerations.[1] The decentralized feedback and feedforward controllers shape the dynamic behavior of the system. In each DOF, the feedback controller consists of a PID structure with an additional low-pass filter, leading to 9.5 Hz bandwidth. The feedback controllers have been designed by applying the sequential loop closing (SLC) loopshaping-based SISO technique on experimentally identified frequency response functions [13]. The SLC method is appropriate when some degree of coupling is still present in the system. The feedforward control action is equal to the reference acceleration times the mass/inertia of the corresponding DOF, which is the optimal action under the rigid-body assumption. When the rigid-body behavior of the motor is actively controlled, the feedback and feedforward blocks compute the desired force/torque vector (1), which should be exerted on the magnet plate [23].

The crucial step for realizing the desired force/torque values is performed in the commutation block. By making use of the electromagnetic relation established in (2), the commutation algorithm computes the currents that will deliver the desired forces and torques. Moreover, the coil switching mechanism, described in Section II-A, is part of the commutation algorithm. In essence, the commutation block decouples and linearizes the position-dependent dynamics that manifest themselves in the input side of the state (3). The so-called direct wrench-current (rigid-body) decoupling commutation method [25], [26] computes the required currents via the following optimization problem

$$\min_{\boldsymbol{i}} ||\boldsymbol{i}||_2^2, \quad \text{subject to} \quad \hat{\boldsymbol{W}} = \hat{M}^{\mathrm{r}}\left(\hat{\boldsymbol{q}}_{\mathcal{T}}^{\mathcal{C}}\right)\boldsymbol{i} \tag{5}$$

where $||\cdot||_2^2$ denotes the squared 2-norm and $\hat{\boldsymbol{W}}$ contains the desired force/torque values (computed by the feedback and feedforward controllers). $\hat{M}^{\mathrm{r}}$ is the estimated value of M^{r}, and it has been computed via numerical integration for each coil and the magnet array on a specified grid of positions [27]. The position $\boldsymbol{q}_{\mathcal{T}}^{\mathcal{C}}$ is estimated by combining the position estimate $\hat{\boldsymbol{q}}_{\mathrm{r}}$ with the metrology-stator position estimate $\hat{\boldsymbol{q}}_{\mathcal{M}}^{\mathcal{C}}$. For the optimization problem (5), under the assumption that $\hat{M}^{\mathrm{r}}$ has full row rank, an analytic solution is derived in the 2-norm optimal sense, (e.g., by least squares [28]) leading to

$$\boldsymbol{i} = \underbrace{\hat{M}^{\mathrm{r}\top}\left(\hat{\boldsymbol{q}}_{\mathcal{T}}^{\mathcal{C}}\right)\left(\hat{M}^{\mathrm{r}}\left(\hat{\boldsymbol{q}}_{\mathcal{T}}^{\mathcal{C}}\right)\hat{M}^{\mathrm{r}\top}\left(\hat{\boldsymbol{q}}_{\mathcal{T}}^{\mathcal{C}}\right)\right)^{-1}}_{\hat{M}^{\mathrm{r}\dagger}\left(\hat{\boldsymbol{q}}_{\mathcal{T}}^{\mathcal{C}}\right)}\hat{\boldsymbol{W}}. \tag{6}$$

By combining (6) and (2), it follows that, if the matrix $\hat{M}^{\mathrm{r}}$ is equal to its true value, M^{r}, the resulting force and torque acting on the mover are equal to the ones computed by the controller. This is made possible by the existence of more actuators, i.e., actively controlled coils, than controlled variables for the rigid body, i.e., the force and torque components.

III. OVERACTUATION APPROACH

In this section, the overactuation scheme is developed for the case of the moving-magnet planar motor, which is based on [6]. Overactuation relies on the existence of additional actuators compared to the controlled variables in the commutation. This property is exploited toward extending (2) to allow for the active control of the flexible behavior of the mover. To this end, the first step is establishing the relation between the force/torque

[1]Under specific assumptions, the position estimation block can be extended to estimate the flexible-body states, too. However in this work the main effort is directed toward suppressing deformations via commutation, instead of directly controlling them by means of feedback control.

components exerted on the individual magnets and the currents in the active coils. As shown in [20] and [27], this relation is described again using the Lorentz force equation. Moreover, it is worth noticing that the torque around each individual magnet contributes to the deformation of the mover by less than 10% [20]. As a result, the effect of the torque components is neglected. In turn, this means that only the relation between the individual magnet forces $\boldsymbol{F}_{\mathrm{M}}$, defined in (3), and the current values has to be established. This relation is described by

$$\boldsymbol{F}_{\mathrm{M}} = \underbrace{\begin{bmatrix} M^{1}_{\mathrm{M}_{1x}}\left(\boldsymbol{q}^{\mathcal{C}}_{\mathcal{T}}\right) & \cdots & M^{n_{\mathrm{c}}}_{\mathrm{M}_{1x}}\left(\boldsymbol{q}^{\mathcal{C}}_{\mathcal{T}}\right) \\ M^{1}_{\mathrm{M}_{1y}}\left(\boldsymbol{q}^{\mathcal{C}}_{\mathcal{T}}\right) & \cdots & M^{n_{\mathrm{c}}}_{\mathrm{M}_{1y}}\left(\boldsymbol{q}^{\mathcal{C}}_{\mathcal{T}}\right) \\ M^{1}_{\mathrm{M}_{1z}}\left(\boldsymbol{q}^{\mathcal{C}}_{\mathcal{T}}\right) & \cdots & M^{n_{\mathrm{c}}}_{\mathrm{M}_{1z}}\left(\boldsymbol{q}^{\mathcal{C}}_{\mathcal{T}}\right) \\ \vdots & \vdots & \vdots \\ M^{1}_{\mathrm{M}_{n_{\mathrm{M}}x}}\left(\boldsymbol{q}^{\mathcal{C}}_{\mathcal{T}}\right) & \cdots & M^{n_{\mathrm{c}}}_{\mathrm{M}_{n_{\mathrm{M}}x}}\left(\boldsymbol{q}^{\mathcal{C}}_{\mathcal{T}}\right) \\ M^{1}_{\mathrm{M}_{n_{\mathrm{M}}y}}\left(\boldsymbol{q}^{\mathcal{C}}_{\mathcal{T}}\right) & \cdots & M^{n_{\mathrm{c}}}_{\mathrm{M}_{n_{\mathrm{M}}y}}\left(\boldsymbol{q}^{\mathcal{C}}_{\mathcal{T}}\right) \\ M^{1}_{\mathrm{M}_{n_{\mathrm{M}}z}}\left(\boldsymbol{q}^{\mathcal{C}}_{\mathcal{T}}\right) & \cdots & M^{n_{\mathrm{c}}}_{\mathrm{M}_{n_{\mathrm{M}}z}}\left(\boldsymbol{q}^{\mathcal{C}}_{\mathcal{T}}\right) \end{bmatrix}}_{M^{\mathrm{M}}\left(\boldsymbol{q}^{\mathcal{C}}_{\mathcal{T}}\right)} \boldsymbol{i} \tag{7}$$

and the magnet force vector is defined as

$$\boldsymbol{F}_{\mathrm{M}} = \begin{bmatrix} F_{\mathrm{M}_{1x}} & F_{\mathrm{M}_{1y}} & F_{\mathrm{M}_{1z}} & \cdots \\ & F_{\mathrm{M}_{n_{\mathrm{M}}x}} & F_{\mathrm{M}_{n_{\mathrm{M}}y}} & F_{\mathrm{M}_{n_{\mathrm{M}}z}} \end{bmatrix}^{\top} \tag{8}$$

where the entry $F_{\mathrm{M}_{n_{\mathrm{M}}x}}$ denotes the force exerted on magnet n_{M} on the x direction, while the rest of the entries in (7) and (8) are defined accordingly. Moreover, $M^{\mathrm{M}}(\boldsymbol{q}^{\mathcal{C}}_{\mathcal{T}}) : \mathbb{R}^{n_{\mathrm{r}}} \mapsto \mathbb{R}^{3n_{\mathrm{M}} \times n_{\mathrm{c}}}$. In the latter matrix, the entry $M^{i}_{\mathrm{M}_{jy}}(\boldsymbol{q}^{\mathcal{C}}_{\mathcal{T}}) : \mathbb{R}^{n_{\mathrm{r}}} \mapsto \mathbb{R}$ denotes the y force component exerted on magnet j by coil i (similarly for the other directions), which depends on the relative position $\boldsymbol{q}^{\mathcal{C}}_{\mathcal{T}}$. At this point, the concept of modal forces is introduced.

Definition III.1 (Modal forces): By making use of (3), (7), and (8), the modal force vector $\boldsymbol{F}_{\mathrm{f}} \in \mathbb{R}^{n_{\mathrm{f}}}$ is defined as

$$\begin{aligned} \boldsymbol{F}_{\mathrm{f}} &= {\Phi^{\mathbb{I}}_{\mathrm{f}}}^{\top} \boldsymbol{F}_{\mathrm{M}} \\ &= {\Phi^{\mathbb{I}}_{\mathrm{f}}}^{\top} M^{\mathrm{M}}\left(\boldsymbol{q}^{\mathcal{C}}_{\mathcal{T}}\right) \boldsymbol{i}. \end{aligned} \tag{9}$$

In essence, each entry of the modal force vector defines a specific force distribution along the magnet plate, which only affects the associated flexible-body state, due to the modal form of the state-space (3). As a consequence, by setting the values of the modal forces, the deformation shape of the magnet plate can be completely specified. In terms of actuation, the latter observation means that the commutation can be appropriately adjusted, so that the computed currents deliver both the desired modal forces $\hat{\boldsymbol{F}}_{\mathrm{f}}$ and the desired rigid-body force and torque vector $\hat{\boldsymbol{W}}$.

It is also worth noticing that, by substituting the rigid-body commutation solution (6) in the modal force (9), under normal operation, the resulting modal forces are nonzero. More importantly, it becomes evident that the modal forces are associated with the controller output $\hat{\boldsymbol{W}}$ in a nonlinear fashion, due to the dependency on the position vector $\boldsymbol{q}^{\mathcal{C}}_{\mathcal{T}}$. As a consequence, the actuation via the rigid-body commutation approach inevitably leads to position-dependent deformations, which is clearly undesirable.

In practice, selecting the desired values for all the modal forces is impossible due to two main reasons. First, for continuous structures, such as the magnet plate, the number of flexible modes is (theoretically) infinite [29], therefore controlling all of them is impossible. Fortunately, since the dynamic response of mechanical structures approximately resembles a low-pass filter, its response can be well approximated by modeling the first few resonances[2], which can then be used in the overactuation scheme. Second, even in the finite order case, it cannot be automatically guaranteed that there is a specific current distribution in (9) that will deliver the desired rigid-body and modal forces. In fact, a necessary condition for the latter is that the number of the controlled variables, i.e., the rigid-body forces/torques and modal forces, is smaller than the number of available coils.

Based on the discussion mentioned above, a selection matrix $S_{\mathrm{f}} \in \mathbb{R}^{n^{\mathbb{I}}_{\mathrm{f}} \times n_{\mathrm{f}}}$ is introduced, which selects the flexible modes in ${\Phi^{\mathbb{I}}_{\mathrm{f}}}^{\top}$ to be actively controlled, together with the rigid-body modes. In analogy to (5), the commutation problem using the overactuation scheme is defined in terms of the minimum 2-norm optimization problem [20], [30]

$$\begin{aligned} &\min_{\boldsymbol{i}} \ ||\boldsymbol{i}||_2^2 \\ &\text{subject to} \begin{bmatrix} \hat{\boldsymbol{W}} \\ \hat{\boldsymbol{F}}_{\mathrm{f}} \end{bmatrix} = \underbrace{\begin{bmatrix} \hat{M}^{\mathrm{r}}\left(\hat{\boldsymbol{q}}^{\mathcal{C}}_{\mathcal{T}}\right) \\ S_{\mathrm{f}} \hat{\Phi}^{\mathbb{I}\top}_{\mathrm{f}} \hat{M}^{\mathrm{M}}\left(\hat{\boldsymbol{q}}^{\mathcal{C}}_{\mathcal{T}}\right) \end{bmatrix}}_{\hat{\Gamma}_{\mathrm{ext}}\left(\hat{\boldsymbol{q}}^{\mathcal{C}}_{\mathcal{T}}\right)} \boldsymbol{i}. \end{aligned} \tag{10}$$

Under the assumption that

$$\operatorname{rank}\left(\hat{\Gamma}_{\mathrm{ext}}\left(\hat{\boldsymbol{q}}^{\mathcal{C}}_{\mathcal{T}}\right)\right) = n_{\mathrm{r}} + n^{\mathbb{I}}_{\mathrm{f}} \tag{11}$$

for which a necessary (but not sufficient) condition is that $n^{\mathbb{I}}_{\mathrm{f}} + n_{\mathrm{r}} \leq n_{\mathrm{c}}$, the least squares solution of (10) is equal to

$$\boldsymbol{i} = \underbrace{\hat{\Gamma}^{\top}_{\mathrm{ext}}\left(\hat{\boldsymbol{q}}^{\mathcal{C}}_{\mathcal{T}}\right)\left(\hat{\Gamma}_{\mathrm{ext}}\left(\hat{\boldsymbol{q}}^{\mathcal{C}}_{\mathcal{T}}\right)\hat{\Gamma}^{\top}_{\mathrm{ext}}\left(\hat{\boldsymbol{q}}^{\mathcal{C}}_{\mathcal{T}}\right)\right)^{-1}}_{\hat{\Gamma}^{\dagger}_{\mathrm{ext}}\left(\hat{\boldsymbol{q}}^{\mathcal{C}}_{\mathcal{T}}\right)} \begin{bmatrix} \hat{\boldsymbol{W}} \\ \hat{\boldsymbol{F}}_{\mathrm{f}} \end{bmatrix}. \tag{12}$$

By combining the commutation solution (12) with the modal force definition in (9) and the rigid body force/torque relation (2), it is straightforward to show that the resulting force distribution on the magnet plate, defined by $\boldsymbol{W}$, $\boldsymbol{F}_{\mathrm{f}}$, is equal to the desired one ($\hat{\boldsymbol{W}}$ and $\hat{\boldsymbol{F}}_{\mathrm{f}}$), if the coefficients in $\hat{\Gamma}_{\mathrm{ext}}$ are equal to the true ones. Therefore, under the latter condition, the overactuation approach (12) can be used to actively control the flexible behavior of the investigated planar motor.

In summary, using the overactuation scheme, the active control of flexible modes is accomplished by controlling the corresponding modal forces. In essence, the main difference between the rigid-body and overactuation-based commutation is that, in the overactuation scheme, not only the total force and torque are specified, but additionally it is specified how these will be distributed on the magnet plate. Therefore, it is also possible to prevent exciting specific modeshapes by setting the corresponding modal forces in (12) to zero. Finally, it is worth noticing that, in order to accomplish the specified force

[2]In fact, such an approximation enabled the derivation of a finite order state-space model in (3).

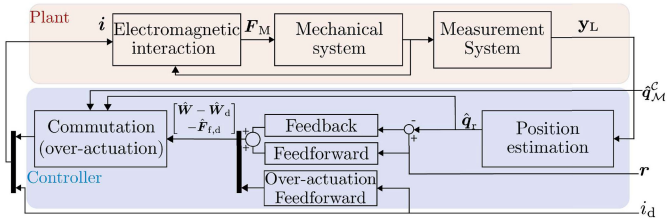

Fig. 5. Block diagram for the DLPM prototype used in the experimental validation of the overactuation scheme.

distribution, the overactuation scheme imposes stricter demands on how the actuation effort must be allocated to the active coils.

IV. Experimental Results

A. Experimental Setting

In this section, the experimental validation of the proposed overactuation scheme is presented. To this end, the DLPM prototype has been utilized. The goal of the followed experimental procedure is to create a deformation-inducing disturbance, which can then be attenuated via the overactuation scheme [22]. To this end, a coil is taken out of the commutation, leaving 39 coils to actively drive the mover. Then, the coil which is left out of the commutation is supplied with a known sinusoidal current signal, denoted by i_{d}, which effectively acts as a disturbance to the system. The frequency of the signal is set to the frequency of a specific flexible mode. Then, by making use of the overactuation scheme, as it has been described in Section III, the effective attenuation of the disturbance-induced spatial deformation is pursued.

The first step toward suppressing the effect of the disturbance current is to estimate its effect in terms of disturbance rigid-body forces/torques and modal forces. For this purpose, the estimated values of the forces, due to the disturbance current, are computed via (2) and (9). With a slight abuse of notation, the columns of $\hat{M}^{\mathrm{r}}$, $\hat{M}^{\mathrm{M}}$, corresponding to the out-of-commutation coil, are denoted by $\hat{M}^{\mathrm{r}}_{\mathrm{d}}$, $\hat{M}^{\mathrm{M}}_{\mathrm{d}}$, while the rest of the 39 columns will be denoted simply by $\hat{M}^{\mathrm{r}}$, $\hat{M}^{\mathrm{M}}$. The position-dependent vectors $\hat{\boldsymbol{W}}_{\mathrm{d}}$, $\hat{\boldsymbol{F}}_{\mathrm{f,d}}$ define the estimated disturbance forces, which must be attenuated via the overactuation scheme. In the performed experiments, the first 4 flexible modes are actively controlled, i.e., $S_{\mathrm{f}} = \begin{bmatrix} I_{4\times 4} & 0_{4\times n_{\mathrm{f}}-4} \end{bmatrix}$. Therefore, the disturbance forces are estimated by

$$\begin{bmatrix} \hat{\boldsymbol{W}}_{\mathrm{d}} \\ \hat{\boldsymbol{F}}_{\mathrm{f,d}} \end{bmatrix} = \begin{bmatrix} \hat{M}^{\mathrm{r}}_{\mathrm{d}}\left(\hat{\boldsymbol{q}}^{\mathcal{C}}_{\mathcal{T}}\right) \\ S_{\mathrm{f}}\hat{\Phi}^{\mathrm{I}^{\top}}_{\mathrm{f}}\hat{M}^{\mathrm{M}}_{\mathrm{d}}\left(\hat{\boldsymbol{q}}^{\mathcal{C}}_{\mathcal{T}}\right) \end{bmatrix} i_{\mathrm{d}}. \tag{13}$$

The attenuation of the disturbance forces is performed by providing the opposite of the forces in (13) by means of a position-dependent feedforward control. The resulting block diagram is shown in Fig. 5. The opposite of the position-dependent matrix in (13) is implemented in the "over-actuation feedforward" block. The resulting force effort is added to the standard rigid-body force/torque vector $\hat{\boldsymbol{W}}$, where the latter is computed by the conventional, rigid-body feedback and feedforward controllers. After defining the required forces, the required current values are computed via (12) and they are subsequently supplied to the active coils. Using this approach, the validity of the proposed scheme is first tested during standstill operation. Then, due to the position dependency of the overactuation scheme, the validity of the proposed scheme is experimentally tested during motion as well.

B. Experimental Validation at Standstill

During standstill operation, the aforementioned experimental procedure has been followed in two different cases. In the first case, the disturbance current has a frequency equal to the first resonance frequency, while in the second case it is equal to the second resonance frequency. The amplitude of the supplied current in both cases is equal to 0.3 A. In each experiment, the position of the magnet plate and the out-of-the-commutation coil have been selected such that the latter coil has the highest coupling to the excited mode. Therefore, it is expected that the resulting deformation shapes on the z-direction will resemble the respective deformation shapes shown in Fig. 4.

For each of the two cases, three different experiments are performed, corresponding to different actuation settings. In Experiment 1, the overactuation approach (12) is used, but all the modal forces and the disturbance current are set to zero. In this way, an estimate for the deformation of the plate due to the noise and the already existing disturbances is derived. In Experiment 2, the disturbance current is supplied to the out-of-commutation coil, but the resulting deformation is not attenuated (the modal force values remain zero). Then, in Experiment 3, the disturbance current is kept on and moreover the overactuation feedforward action based on (13) is enabled, as it was described in Section IV-A.

The deformation of the magnet plate has been measured using the 25 z-axis LIFM system, as shown in Fig. 1. The data are captured using a sampling frequency $F_{\mathrm{s}} = 10\,\mathrm{kHz}$. In each performed experiment data are captured for 6 s, leading to $N = 6 \cdot 10^4$ datapoints per LIFM. The derived measurements are postprocessed to allow for the better interpretation of the results, by focusing on the deformation of the plate instead of any rigid-body displacements and rotations. To this end, for each time instant, the average z displacement of the 25 LIFMs is computed and removed from each measurement signal. Then, a flat surface is fitted and subtracted from the measured surface, such that the effect of rotations is removed. Finally, the signals are filtered using a bandpass filter, with lower and upper cutoff frequencies equal to 100 and 1500 Hz, respectively. In order to quantify the level of deformation, the sum of the ℓ_2 norms of the resulting measurements is computed, scaled by the total number of datapoints

$$e_{\ell_2} = \sqrt{\sum\nolimits_{i=1}^{25} ||\mathbf{y}_i||_2^2 / (25N)} \tag{14}$$

with $\mathbf{y}_i \in \mathbb{R}^N$ representing the N measurements from the ith auxiliary LIFM device. The results are shown in Table II. In this table the relative reduction of the deformations in Experiment 3 with respect to Experiment 2 has been computed, too. To account for the noise level in each experiment, the corresponding norm values from Experiment 1 are subtracted from Experiments 2

TABLE II
EXPERIMENTAL RESULTS DURING STANDSTILL, ℓ_2-BASED NORM

# Flexible mode	Exp. 1 [nm]	Exp. 2 [nm]	Exp. 3 [nm]	Relative reduction [%]
1^{st}	0.07	82.13	8.36	89.90
2^{nd}	0.82	64.65	7.59	89.39

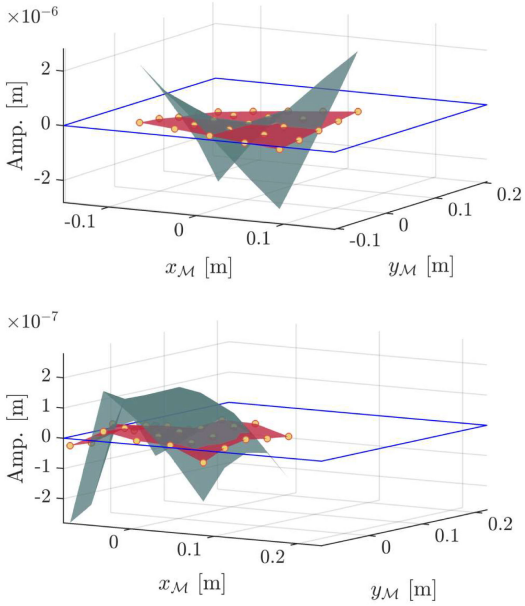

Fig. 6. Experimental results using overactuation. Maximum displacement due to deformation under disturbance (▬, Experiment 2) and under disturbance and feedforward compensation (▬, Experiment 3) are plotted. The circles at the plot of Experiment 3 depict the location of the 25 sensors. The blue line depicts the edges of the top mirror. Top: first flexible mode. Bottom: second flexible mode.

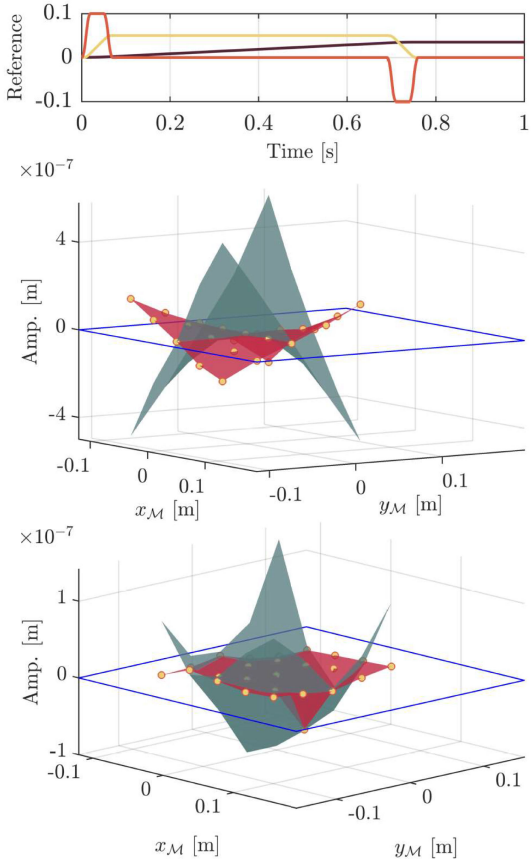

Fig. 7. Experimental results using overactuation. Top plot: Position (▬), velocity (▬), and acceleration scaled by 10 (▬) profile in x-direction. Bottom two plots: Maximum displacement due to deformation under disturbance (▬, Experiment 2) and under disturbance and feedforward compensation (▬, Experiment 3) are plotted. The circles at the plot of Experiment 3 depict the location of the 25 sensors. The blue line depicts the edges of the top mirror. Middle plot: first flexible mode. Bottom plot: second flexible mode.

and 3. Therefore, the relative reduction using the ℓ_2 norm is computed by

$$\text{relative reduction } \% = \left| \frac{e_{\ell_2}\,(\text{Exp. 2}) - e_{\ell_2}\,(\text{Exp. 3})}{e_{\ell_2}\,(\text{Exp. 2}) - e_{\ell_2}\,(\text{Exp. 1})} \right| \cdot 100\%. \tag{15}$$

Moreover, in Fig. 6, the worst-case deformations are shown for the Experiments 2 and 3.

Based on these experimental results, it is verified that in both experimental cases the resulting deformation shapes, shown in Fig. 6, correspond to the ones predicted by the developed multiphysical model, as shown in Fig. 4. More importantly, it is concluded that the proposed overactuation scheme is capable of describing and successfully attenuating the introduced disturbance. This is verified by the percentage-wise relative reduction of the deformation, which is approximately equal to 90% for both investigated flexible modes.

C. Experimental Validation Under Motion

In this section, the verification of the proposed overactuation scheme during motion is performed. The experimental settings that have been used during standstill experiments are used here, too. However, in the experiments of this section, the magnet plate follows a fourth-order trajectory [31], as shown in Fig. 7. In order to reduce the effect of external disturbances associated with large force values, the maximum trajectory speed and acceleration have been set to $0.05\,\text{m/s}$ and $1\,\text{m/s}^2$, respectively. The exact same procedure has been used for filtering the resulting LIFM data, as the one described in Section IV-B. The experimental results for the first two flexible modes are shown in Fig. 7. Moreover, in Table III, the quantitative comparison of the resulting deformations is presented.

TABLE III
EXPERIMENTAL RESULTS DURING MOTION, ℓ_2-BASED NORM

# Flexible mode	Exp. 1 [nm]	Exp. 2 [nm]	Exp. 3 [nm]	Relative reduction [%]
1^{st}	41.46	91.96	68.57	46.32
2^{nd}	26.16	47	26.73	97.26

Similar to the standstill results, in the moving case, it is concluded that the overactuation scheme manages to suppress the induced disturbance. Especially for the second mode, the overactuation can almost fully reject the disturbance. For the first flexible mode, the improvement is less pronounced, but at the same time, the estimated level of noise and inherent disturbances (Experiment 1) is significantly higher than the corresponding

estimate for the second mode. In general, for both flexible modes, the deformation of the magnet plate under Experiment 1 is much higher compared to the standstill case, thus hinting at the more challenging nature of the experiments under motion. In total, though, these results confirm that the overactuation approach can efficiently cope with the position-dependent dynamics that are present in the planar motor system and attenuate the disturbance-induced deformations.

V. Conclusion

In this article, an overactuation technique has been developed for a magnetically levitated planar motor. The overactuation method is based on the description of the deformation shape in terms of individual elementary motions (modes), and the subsequent active control of the selected flexible modes. To this end, the method makes use of both the position-dependent electromagnetic and motion dynamics models. The overactuation scheme has been experimentally evaluated toward the compensation of an applied current disturbance by means of feedforward control, under both standstill and trajectory tracking cases. The derived results verified the validity of the proposed method, showing that even a nearly complete rejection of the induced disturbance can be accomplished.

In total, the value of the proposed overactuation approach is twofold. First, by actively controlling the modal forces via the overactuation scheme, the (unintended) excitation of the flexible dynamics is avoided, which was indeed the case under the rigid-body commutation scheme. Second, the proposed approach paves the road toward active compensation of disturbances that act on the system, which was experimentally verified in this publication through the use of feedforward control. Finally, the overactuation approach can be further exploited by making use of the estimated flexible states in a feedback loop, in parallel to the currently implemented feedback loop for the rigid-body states.

References

[1] R. H. M. Schmidt, "Ultra-precision engineering in lithographic exposure equipment for the semiconductor industry," *Philos. Trans. Roy. Soc. A: Math., Phys. Eng. Sci.*, vol. 370, no. 1973, pp. 3950–3972, 2012.

[2] K. Ki-Hyun *et al.*, "Design of decoupled dual servo stage with voice coil motor and linear motor for XY long stroke ultra-precision scanning system," *Proc. SPIE*, vol. 6040, pp. 273–278, 2006.

[3] J. C. Compter, "Electro-dynamic planar motor," *Precis. Eng.*, vol. 28, no. 2, pp. 171–180, 2004.

[4] H. Zhu, T. J. Teo, and C. K. Pang, "Design and modeling of a six-degree-of-freedom magnetically levitated positioner using square coils and 1-D halbach arrays," *IEEE Trans. Ind. Electron.*, vol. 64, no. 1, pp. 440–450, Jan. 2017.

[5] L. Xiaodong and I. Usman, "6D direct-drive technology for planar motion stages," *CIRP Ann.*, vol. 61, no. 1, pp. 359–362, 2012.

[6] J. M. M. Rovers, J. W. Jansen, and E. A. Lomonova, "Design and measurements of the double layer planar motor," in *Proc. IEEE Int. Electric Mach. Drives Conf.*, 2013, pp. 204–211.

[7] J. M. M. Rovers, J. W. Jansen, and E. A. Lomonova, "Multiphysical analysis of moving-magnet planar motor topologies,"*IEEE Trans. Magn.*, vol. 49, no. 12, pp. 5730–5741, Dec. 2013.

[8] J. W. Jansen, "Magnetically levitated planar actuator with moving magnets: Electromechanical analysis and design i," Ph.D. dissertation, Electromechanics Power Elect., Eindhoven Univ. Technol., Eindhoven, The Netherlands, 2007.

[9] R. van Herpen, T. Oomen, E. Kikken, M. van de Wal, W. Aangenent, and M. Steinbuch, "Exploiting additional actuators and sensors for nano-positioning robust motion control," *Mechatronics*, vol. 24, no. 6, pp. 619–631, 2014.

[10] T. Oomen, R. van Herpen, S. Quist, M. van de Wal, O. Bosgra, and M. Steinbuch, "Connecting system identification and robust control for next-generation motion control of a wafer stage," *IEEE Trans. Control Syst. Technol.*, vol. 22, no. 1, pp. 102–118, Jan. 2014.

[11] J. Rovers *et al.*, "The deformation of the moving magnet plate of a commutated magnetically levitated planar actuator," *Mechatronics*, vol. 23, no. 2, pp. 233–239, 2013.

[12] R. Voorhoeve, R. de Rozario, W. Aangenent, and T. Oomen, "Identifying position-dependent mechanical systems: A modal approach applied to a flexible wafer stage," *IEEE Trans. Control Syst. Technol.*, vol. 29, no. 1, pp. 194–206, Jan. 2021.

[13] M. Steinbuch, R. Merry, M. Boerlage, M. Ronde, and M. van de Molengraft, *Advanced Motion Control Design*. Boca Raton, FL, USA: CRC Press, 2010, pp. 27–1/25.

[14] W. Gawronski, *Advanced Structural Dynamics and Active Control of Structures*. Berlin, Germany: Springer, 2004.

[15] M. Schneiders, M. van de Molengraft, and M. Steinbuch, "Introduction to an integrated design for motion systems using over-actuation," in *Proc. Eur. Control Conf.*, 2003, pp. 3249–3254.

[16] M. G. E. Schneiders, M. J. G. van de Molengraft, and M. Steinbuch, "Benefits of over-actuation in motion systems," in *Proc. Amer. Control Conf.*, Jun. 2004, vol. 1, pp. 505–510.

[17] S. D. Galvan, M. Heertjes, and R. Dunand, "Plant enhancements in motion systems by modal control," in *Proc. Amer. Control Conf.*, 2012, pp. 5348–5353.

[18] M. Ronde, G. Leenknegt, M. van de Molengraft, and M. Steinbuch, "Data-based spatial feedforward for over-actuated motion systems," *Mechatronics*, vol. 24, no. 6, pp. 679–690, 2014.

[19] M. Ronde, M. Schneiders, E. Kikken, M. van de Molengraft, and M. Steinbuch, "Model-based spatial feedforward for over-actuated motion systems," *Mechatronics*, vol. 24, no. 4, pp. 307–317, 2014.

[20] J. M. M. Rovers, "Multiphysical modeling of high-precision electromechanical devices," Ph.D. dissertation, Electromechanics Power Elect., Eindhoven Univ. Technol., Eindhoven, The Netherlands, 2013.

[21] J. M. M. Rovers, J. W. Jansen, J. C. Compter, and E. A. Lomonova, "Analysis method of the dynamic force and torque distribution in the magnet array of a commutated magnetically levitated planar actuator," *IEEE Trans. Ind. Electron.*, vol. 59, no. 5, pp. 2157–2166, May 2012.

[22] C. Custers *et al.*, "Active compensation of the deformation of a magnetically levitated mover of a planar motor," in *Proc. IEEE Int. Electric Mach. Drives Conf.*, 2019, pp. 854–861.

[23] I. Proimadis, "Nanometer-accurate motion control of moving-magnet planar motors," Ph.D. dissertation, Dept. Elect. Eng., Technische Universiteit Eindhoven, Eindhoven, The Netherlands, 2020.

[24] *ANSYS Academic Research Mechanical*, *Release 17.1*, ANSYS Inc., Canonsburg, PA, USA, 2016.

[25] C. H. H. M. Custers, J. W. Jansen, and E. A. Lomonova, "Static decoupling of force and torque components in a moving-magnet planar motor," in *Proc. IEEE Int. Electric Mach. Drives Conf.*, May 2017, pp. 1–8.

[26] J. Jansen, E. Lomonova, A. Damen, P. van denBosch, and A. Vandenput, "Commutation of a magnetically levitated planar actuator with moving-magnets," *IEEJ Trans. Ind. Appl.*, vol. 128, no. 12, pp. 1333–1338, 2008.

[27] C. Custers, "Overactuated magnetically levitated systems: Flexible modes and eddy current phenomena in high-precision bearingless planar motors," Ph.D. dissertation, Electromechanics Power Elect., Eindhoven Univ. Technol., Eindhoven, The Netherlands, 2019.

[28] G. Golub and C. van Loan, *Matrix Computations*, 4th ed. Baltimore, MD, USA: The Johns Hopkins University Press, 2013.

[29] P. Hughes, "Space structure vibration modes: How many exist? which ones are important?" *IEEE Control Syst. Mag.*, vol. 7, no. 1, pp. 22–28, Feb. 1987.

[30] J. W. Jansen, J. P. C. Smeets, T. T. Overboom, J. M. M. Rovers, and E. A. Lomonova, "Overview of analytical models for the design of linear and planar motors," *IEEE Trans. Magn.*, vol. 50, no. 11, Nov. 2014, Art. no. 8206207.

[31] P. Lambrechts, M. Boerlage, and M. Steinbuch, "Trajectory planning and feedforward design for electromechanical motion systems," *Control Eng. Pract.*, vol. 13, no. 2, pp. 145–157, 2005.